

Self-assembly of binary nanoparticles on soft elastic shells

Yangwei Jiang, Dong Zhang, Yankang Jin, and Linxi Zhang

Citation: *J. Chem. Phys.* **138**, 214901 (2013); doi: 10.1063/1.4807592

View online: <http://dx.doi.org/10.1063/1.4807592>

View Table of Contents: <http://jcp.aip.org/resource/1/JCPSA6/v138/i21>

Published by the AIP Publishing LLC.

Additional information on J. Chem. Phys.

Journal Homepage: <http://jcp.aip.org/>

Journal Information: http://jcp.aip.org/about/about_the_journal

Top downloads: http://jcp.aip.org/features/most_downloaded

Information for Authors: <http://jcp.aip.org/authors>

ADVERTISEMENT



Explore the **Most Cited**
Collection in Applied Physics

AIP
Publishing

Self-assembly of binary nanoparticles on soft elastic shells

Yangwei Jiang,¹ Dong Zhang,¹ Yankang Jin,¹ and Linxi Zhang^{2,a)}

¹Department of Physics, Zhejiang University, Hangzhou 310027, China

²Department of Physics, Wenzhou University, Wenzhou 325035, China

(Received 22 February 2013; accepted 9 May 2013; published online 4 June 2013)

The self-assembly behaviors and phase transitions of binary nanoparticles (NPs) adsorbed on a soft elastic shell are investigated through molecular dynamics simulation. The conformations of adsorbed binary NPs depend on the bending energy K_b of elastic shell and the binding energy D_0 between the NPs and the elastic shell. The ordered structures of binary NPs are observed at the moderate adhesive strength and bending energy, in which the small NPs are located near the vertices of regular pentagons as well as the large NPs are distributed along the sides of the regular pentagons. The shape of soft elastic shell can be adjusted by adding the adsorbed binary NPs, and this investigation can provide an effective way to regulate and reshape surfaces or membranes with the sizes in the micrometer range or smaller. © 2013 AIP Publishing LLC. [<http://dx.doi.org/10.1063/1.4807592>]

I. INTRODUCTION

Molecular self-assembly plays an important role in patterning matter on the atomic scale, and it has seen advances in the development of methods for designing self-assembling biomaterial and nanomaterial. Trimeric proteins into a desired symmetric structure,^{1,2} pH-induced self-assembly of peptide-amphiphile into nanofibers,³ nanoparticle (NP) phospholipid bilayer disks packed by membrane scaffold proteins and phospholipid,⁴ and aggregation of colloidal nanoparticles into crystalline⁵ are the typical examples of self-assembly processes. A good understanding of the self-assembly of biological and artificial components will reveal critical biological and physical processes, and holds promise in the regulation and shaping of nanomaterial in the micrometer range or smaller size.

Particles at interfaces can be used to study some basic problems in condensed matter physics, such as the physical behavior of two-dimensional crystals.^{6–9} The fluid interface has revolutionized the field of self-assembly by providing a universal mechanism through which arbitrary building blocks can be driven close to each other. When hard particles without interaction bind to a deformable elastic shell, the morphology of the patterns can be controlled by the mechanical properties of the surface and the strength of the particle adhesion.^{10–14} For instance, hard NPs adsorbed on a deformable elastic shell are likely to self-assemble into a variety of linear patterns.¹⁰ The nontrivial elastic response to the deformation of soft elastic surfaces can lead to anisotropic interactions between the particles resulting in the aggregates having different geometrical features.¹¹ With the help of curvature-mediated interactions, spherical NPs adhering to the outer surface of a deformable nanotube can self-assemble into linear structures,¹² and fluid membranes can mediate linear aggregation structures of adsorbed NPs.¹⁴ The ordered regular pentagons of polymers binding to an elastic shell are also observed at the

moderate adhesive strength and bending energy.¹⁵ In addition, several experimental studies of NPs at interfaces have reported the formation of unusual structures,^{16,17} motivating new theoretical approaches to colloidal interactions beyond the traditional bulk considerations.^{6,18} The experimental results show that silver passivated NPs at the air-water interface spontaneously can form clusters and stripelike arrays.¹⁶ NPs at fluid interfaces are becoming a central topic in colloid science studies,^{6,18} and the small size of NPs leads to a weak confinement of the NPs at the fluid interface that can provide size-selective particle assembly, two-dimensional phase behavior, and functionalization.¹⁹ However, almost all the works mentioned above are focused on only one kind of NPs, considering the fact that the binary NPs can exhibit very rich phase diagrams with multiple close-packed and non-close-packed phases, such as crystallization of NPs,^{20–23} superlattice structures,^{24–26} glass transition,^{27–30} it is also very important to study the conformations of the binary NPs. The NPs of different metals, semiconductors, and magnetic materials can self-assemble from colloidal solutions into long-range-ordered periodic structures.²⁴ The self-assembly of a binary mixture of nanoparticles in ionic liquid-in-water pickering emulsions is reported, with emphases on the interfacial self-assembled nanoparticle structure and the partitioning preference of free nanoparticles in the dispersed and continuous phases.³¹ Therefore, the binary NPs system may promise a new approach for controlling the self-assembling behavior of NPs at atomic accuracy and constructing a better macroscopic performance of the material. In this paper, the self-assembly behaviors of binary NPs adsorbed on soft elastic shells are investigated by using molecular dynamics simulation, and ordered structures of adsorbed binary NPs on elastic shells are observed at the moderate binding energy and bending energy.

II. MODEL

The elastic surface is modeled by employing the fishnet-like network, in which the bead positions on the elastic

^{a)} Author to whom correspondence should be addressed. Electronic mail: lxzhang@zju.edu.cn.

surface are determined by triangulation.³² In order to prevent overlap between any two surface beads, the beads undergo the interactions of a purely repulsive truncated and shifted Lennard-Jones potential with each other

$$U_{\text{LJ}}(r) = \begin{cases} 4\varepsilon \left[\left(\frac{\sigma}{r} \right)^{12} - \left(\frac{\sigma}{r} \right)^6 + \frac{1}{4} \right], & r \leq 2^{1/6}\sigma \\ 0, & r > 2^{1/6}\sigma \end{cases}, \quad (1)$$

where r refers to the distance between the centers of any two surface beads, σ is the bead diameter, and $\varepsilon = 1.0 k_B T$.

Each pair of adjacent beads on the surface joins together through a finite extensible nonlinear elastic (FENE) spring potential to guarantee the connectivity of the elastic surface

$$U_{\text{FENE}}(r) = -\frac{K l_0^2}{2} \ln \left[1 - \left(\frac{r}{l_0} \right)^2 \right], \quad r < l_0, \quad (2)$$

where two constants in this potential function are set as $K = 30 k_B T / \sigma^2$ and $l_0 = 3\sigma$.

The bending rigidity of the elastic surface is modeled by a dihedral potential between adjacent triangles,^{13,15}

$$U_{\text{bending}} = K_b (1 + \cos \phi), \quad (3)$$

where ϕ is the dihedral angle between opposite vertices of any two triangles sharing an edge and K_b refers to the bending energy constant.

To avoid overlap, the repulsive truncated-shifted Lennard-Jones potential written in Eq. (1) is also applied to the binary NPs with the radius of large NPs $\sigma_l = 5.0\sigma$ and the radius of small NPs $\sigma_s = 2.5\sigma$, and the parameters are given by the mixing rules: $\varepsilon_{ij} = \sqrt{\varepsilon_i \varepsilon_j} = \varepsilon$ and $\sigma_{ij} = (\sigma_i + \sigma_j)/2$ ($i, j = l, s$). A Morse potential is adopted to characterize the binding energy strength between binary NPs and the elastic shell

$$U_{\text{Morse}}(r) = \begin{cases} \varepsilon_M (e^{-2\alpha(r-r_{nm})} - 2e^{-\alpha(r-r_{nm})}), & r \leq 10\sigma \\ 0, & r > 10\sigma \end{cases}, \quad (4)$$

where ε_M is the attractive interaction strength, r refers to the center-to-center distance between a NP and a surface-bead, and $r_{nm} = (\sigma + \sigma_i)/2$ ($i = l, s$) denotes the equilibrium distance of a surface-beads and a NP. Moreover, the interaction cutoff is fixed to be 10σ and $\alpha = 1.25/\sigma$ is chosen.

We employ the LAMMPS molecular dynamics package³³ with a Nosé-Hoover thermostat^{34,35} in the NVT ensemble to study the self-assembly behavior of binary NPs adsorbed on a soft elastic shell. The temperature is set to $T = 1.0$, the timestep is $\tau = 0.001\tau_0$ and each simulation runs at least 5×10^7 steps in the periodic box $200\sigma \times 200\sigma \times 200\sigma$. Meanwhile, the number of the surface-beads is $N_b = 10\,242$ for $R = 26.4\sigma$. We have checked the influence of finite size by choosing a large periodic box of $300\sigma \times 300\sigma \times 300\sigma$ as well as the influence of the size of elastic shell through using a new shell model built by 40 962 beads with $R = 48.6\sigma$, and the similar results are also observed (see Figures S1 and S2 in the supplementary material³⁶). Therefore, the effects of finite size of periodic box and the size of elastic shell can be ignored.

III. RESULTS AND DISCUSSION

A. Self-assembly structures for binary NPs

The deformation of elastic shell and the aggregation structures of binary NPs depends simultaneously on the bending energy K_b and the binding energy D_0 , and it is schematically depicted in Fig. 1. Here the numbers of large NPs (N_L) and small NPs (N_S) are fixed, i.e., $N_L = N_S = 60$. For the high binding energy and the low bending energy, such as $D_0 = 50$ and $K_b = 500$, the elastic shell is quite soft and has a large deformation, as well as the NPs have low mobility. With the decrease of binding energy D_0 and the increase of bending energy K_b , such as $D_0 = 35$ and $K_b = 1000$, an ordered regular pentagons is formed, in which the small NPs are located around the vertices of regular pentagons and the large NPs are distributed along the sides of regular pentagons. In fact, these binary NPs on the elastic shell can self-assemble into the framework of a dodecahedron, which is in good agreement with the Cacciuto's result of the single NPs on elastic shell.¹⁰ When the binding energy decreases further or the bending energy increases a little, such as $D_0 = 25$ and $K_b = 2000$, the ordered structure of binary NPs is destroyed partly. Since the decrease of binding energy can weaken the control of binary NPs and strengthen the mobility of binary NPs, the semi-ordered structure is presented. When the bending energy continues to increase, it can drive the binary NPs to aggregate into the clusters, especially for the small NPs. Of course, when the bending energy increases further, the elastic shell becomes a hard sphere gradually, and the binary NPs can aggregate into clusters at the high binding energy such as $K_b = 30\,000$, in which small NPs locate on the valley regions of the elastic shell with large NPs around them.

The ordered structure of binary NPs can be explored through calculating the average number of small NPs around the vertices of pentagons $\langle n_S \rangle$ and the average number of large NPs distributed along the sides of pentagons $\langle n_L \rangle$, as well as their fluctuations of $\langle n_S^2 \rangle - \langle n_S \rangle^2$ and $\langle n_L^2 \rangle - \langle n_L \rangle^2$,

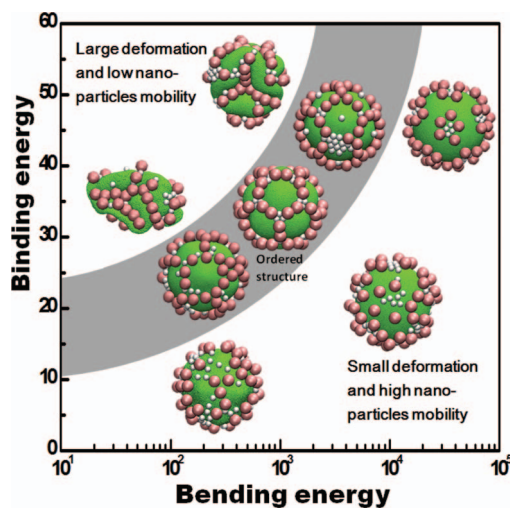


FIG. 1. Phase diagram indicating the conformations of adsorbed binary NPs and the shapes of elastic shells are controlled by the bending energy K_b and the binding energy D_0 . Binary NPs can self-assemble into ordered regular pentagons at the moderate adhesive strength and bending energy.

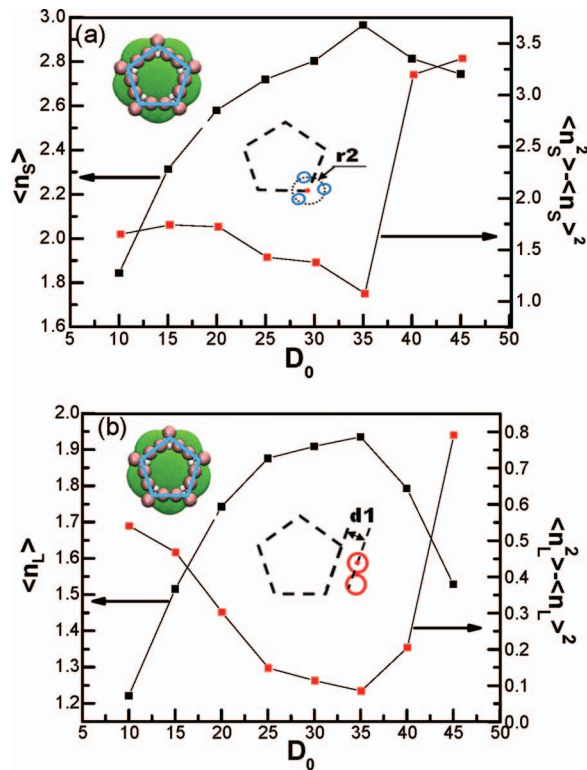


FIG. 2. (a) The average number of small NPs around the vertices of pentagons $\langle n_S \rangle$ and its fluctuation $\langle n_S^2 \rangle - \langle n_S \rangle^2$; (b) the average number of large NPs along the sides of pentagons $\langle n_L \rangle$ and its fluctuation $\langle n_L^2 \rangle - \langle n_L \rangle^2$ as a function of the binding energy D_0 . Here $K_b = 1000$.

and the results are shown in Figs. 2(a) and 2(b), respectively. Here the numbers of large NPs and small NPs are fixed, i.e., $N_L = N_S = 60$. When the binding energy D_0 increases from 10 to 35, the conformations of adsorbed binary NPs change from the collapsed structure or the semi-ordered structure to the ordered regular pentagon. The average number of small NPs $\langle n_S \rangle$ increases from $\langle n_S \rangle = 1.84$ – 2.97 at $D_0 = 35$. Here the value of r_2 is selected as 6.0, see the inset of Fig. 2(a). In the perfect case, each dodecahedron has 12 pentagons sharing 30 sides and 20 vertices, therefore, the theoretical value of $\langle n_S \rangle$ is $\langle n_S \rangle_T = \frac{60}{20} = 3.0$. At the same time, a small fluctuation value of $\langle n_S^2 \rangle - \langle n_S \rangle^2$ means that the distribution of small NPs is uniform, and the conformation of small NPs is the ordered structure. In fact, when the small NPs are located near the vertices, the large NPs have to be distributed along the sides of pentagons. Therefore, we also calculate the average number of large NPs distributed along the sides of pentagons $\langle n_L \rangle$ and its fluctuation of $\langle n_L^2 \rangle - \langle n_L \rangle^2$. Here $d_1 = 9$ is selected. When the binding energy D_0 increases, $\langle n_L \rangle$ increases first and then it approaches to the maximum value of $\langle n_L \rangle = 1.94$ at $D_0 = 35$, which is close to the theoretical value of $\langle n_L \rangle_T = \frac{60}{30} = 2.0$ because each dodecahedron has 30 sides, while the fluctuation value of $\langle n_L^2 \rangle - \langle n_L \rangle^2$ decreases and it is close to the minimum value at $D_0 = 35$. Meanwhile, if the binding energy increases further, the ordered regular structure will be destroyed and the binary NPs move towards the “valley” regions of elastic shell (i.e., the vertices of pentagons of elastic shell), so both $\langle n_S \rangle$ and $\langle n_L \rangle$ decrease, while their fluctuation values of $\langle n_S^2 \rangle - \langle n_S \rangle^2$ and $\langle n_L^2 \rangle - \langle n_L \rangle^2$ in-

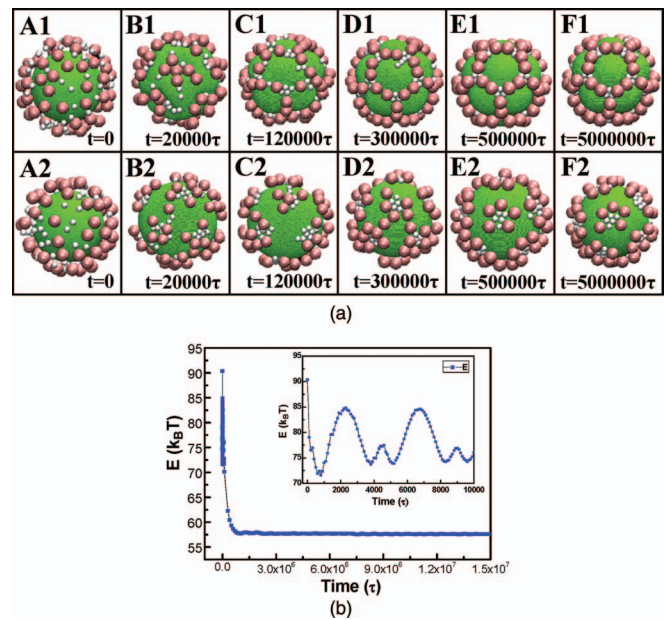


FIG. 3. (a) Snapshots at different simulation time suggesting the formation of an ordered structure at weak bending energy of $K_b = 1000$ (A1)–(F1) and the aggregation structure at strong bending energy of $K_b = 20000$ (A2)–(F2) with the binding energy of $D_0 = 35$. (b) The total energy of the system for the elastic shell with $K_b = 20000$ and $D_0 = 35$ as a function of the iteration step.

crease. The transition from the semi-ordered conformations to the ordered regular pentagons is achieved by varying the binding energy, and the aggregation structures depend on the bending energy and the binding energy simultaneously. The largest values of $\langle n_S \rangle$ and $\langle n_L \rangle$ with the smallest fluctuations at $D_0 = 35$ indicate that there exist the ordered structures at the moderate binding energy and bending energy.

To understand the mechanism of forming ordered aggregation structures of binary NPs, we explore the simulation processes of system with two different bending energies $K_b = 1000$ and $K_b = 20000$, and the results are shown in Fig. 3. At first, the binary NPs are placed randomly in the simulation box and away from the elastic shell. After a short simulation time, the binary NPs are adsorbed uniformly on the elastic shell under the effects of binding energy. Then, both the small and the large NPs move towards the flat area of elastic shells and these movements can minimize the total system energy. Moreover, the small NPs have advantages over the large NPs in the competition of taking over the flat area. For the case of $K_b = 1000$, small NPs prefer to stay the vertices of pentagons, while the large NPs tend to aggregate along the sides. The “peaks” of elastic shell help to hold the large NPs alone and prevent them from moving to the vertices of pentagons. The small NPs can still adjust their position by moving from one vertex to another. After a long period of equilibrium, ordered regular pentagons are finally formed, see Fig. 3(a)(F1). For the another case of $K_b = 20000$, the binary NPs first aggregate into clusters and small NPs take over the center of the clusters surrounded by large NPs. Small NPs stay in the centers of the clusters earlier, while large NPs move from one cluster to another to minimize the total system energy, which is in accordance with the aggregation behaviors of single NPs

on the hard spheres.^{37,38} As shown in Fig. 3(b), with the increase of the iteration step, the total energy E of the system decreases rapidly and the system reaches equilibrium after $t = 1.5 \times 10^6 \tau$. Here the total potential energy E includes Lennard-Jones potential energy U_{LJ} , FENE spring potential energy U_{FENE} , the bending energy $U_{bending}$, and the Morse potential energy U_{Morse} .

In order to have a better understanding of the aggregation structures of binary NPs and find out the physical origin of different conformations of binary NPs, we describe those conformations in the spherical coordinate system (R, Θ, Φ) instead of Cartesian coordinate system (x, y, z) , and the values of R , Θ , and Φ can be determined by

$$x_i = R_i \sin \Theta_i \cos \Phi_i, \quad (5)$$

$$y_i = R_i \sin \Theta_i \sin \Phi_i, \quad (6)$$

$$z_i = R_i \cos \Theta_i. \quad (7)$$

The radius distributions $R = R(\Theta, \Phi)$ as a function of Θ , and Φ with two different bending energies $K_b = 1000$ and $20\,000$ are shown in Fig. 4(a). The radius distributions of soft elastic shells with $K_b = 1000$ and $20\,000$ in the absence of

adsorbed binary NPs are given in Figs. 4(a)(I) and 4(a)(IV). For the soft elastic shell with weak bending energy of $K_b = 1000$, there are a series of peaks on the $\Theta\Phi$ -surface (see Fig. 4(a)(I)). The area of each peak and the distance between any two neighboring peaks are the same, and the number of peaks is 12. Meanwhile, there are some valleys on the $\Theta\Phi$ -surface, and the number of valleys (or the vertices of pentagons) is 20. When the elastic shell is binding with binary NPs, the effects of adsorbed binary NPs on the radius distribution are obvious. The peaks on the $\Theta\Phi$ -surface become sharper, see Fig. 4(a)(II). As small NPs occupy less areas than large NPs on the $\Theta\Phi$ -surface, the equilibrium state in which small NPs are located at the vertices of pentagons with large NPs around them is stable state, see Fig. 4(b)(I). If large NPs are located the valley regions, this is the unstable state, see Fig. 4(b)(II). For the hard elastic shell with high bending energy of $K_b = 20\,000$, as the bending energy is larger than the stretching energy,¹⁰ the shape of elastic shell is determined mainly by the bending energy and the radius distributions of elastic shell with $K_b = 20\,000$ are completely different from the elastic shell with $K_b = 1000$,¹⁵ see Fig. 4(a)(IV). The peak regions of radius distributions for elastic shell with $K_b = 1000$ become the valley regions for elastic shell with $K_b = 20\,000$.¹⁵ Therefore, the aggregation clusters of binary NPs are distributed among those 12 regions, in which small NPs are surrounded by large NPs, see Fig. 4(a)(VI). By taking into account of the position distributions of small and large NPs (see Figs. 4(a)(III) and 4(a)(VI)), we find that the binary NPs would like to stay at the small radius region to minimize the total system energy because a small deformation of elastic shell can produce a little bending energy, which corresponds to the flat area on the elastic surface. As small NPs occupy less area than large NPs, small NPs have to stay the center of “valley,” and small NPs play a more important role in the aggregation of binary NPs. Of course, if the binary NPs are adsorbed on the *hard* surface, we *suppose* that the free volume framework may be employed to account for the mechanisms of aggregation of binary NPs.^{39,40}

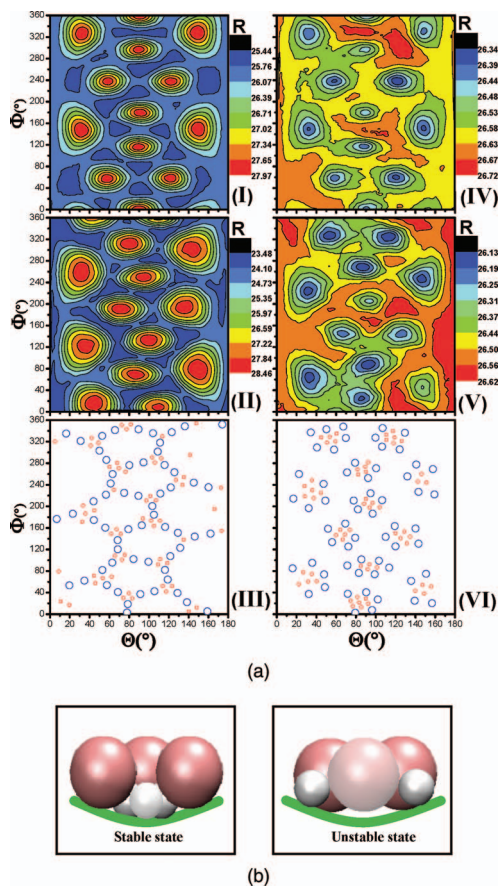


FIG. 4. (a) The radius distributions of elastic shells with $D_0 = 35$, $N_S = 60$, $N_L = 60$, $K_b = 1000$ (left), and $K_b = 20\,000$ (right) on the $\Theta\Phi$ -surface. From top to bottom: the radius distribution of the free elastic shell, the radius distribution of the elastic shell in the presence of adsorbed binary NPs, and the position distribution of adsorbed binary NPs. (b) Two typical states show that for the stable state, the small NPs are located on the “valleys” of elastic shell with large NPs around them.

B. Effects of binary NPs on the shape of elastic shell

When we change the total number of binary NPs for an elastic shell at the moderate adhesive strength, such as $D_0 = 15$ and $K_b = 300$, another interesting phenomenon is observed, and the results are given in Fig. 5(a). When the total number of binary NPs increases, elastic shell undergoes a process from a sphere (see Fig. 5(a)(a1)), to a collapsed shell (see Fig. 5(a)(a2)), and back to a sphere (see Fig. 5(a)(a4)). In order to take a clear look of elastic shell, we make the NPs invisible in Fig. 5(b).

When 1 large NP and 3 small NPs are adsorbed on the soft elastic shell (i.e., $N_L/N_S = 1/3$), the weak deformation of soft elastic shell occurs (see Fig. 5(b)(a1)). When the total number of binary NPs increases to $N_L + N_S = 200$ with the same proportion of $N_L/N_S = 1/3$, the soft elastic shell is collapsed completely and is folded into several layers, as shown in Fig. 5(b)(a2). However, if the total number of binary NPs increases further to $N_L + N_S = 400$, only local collapse

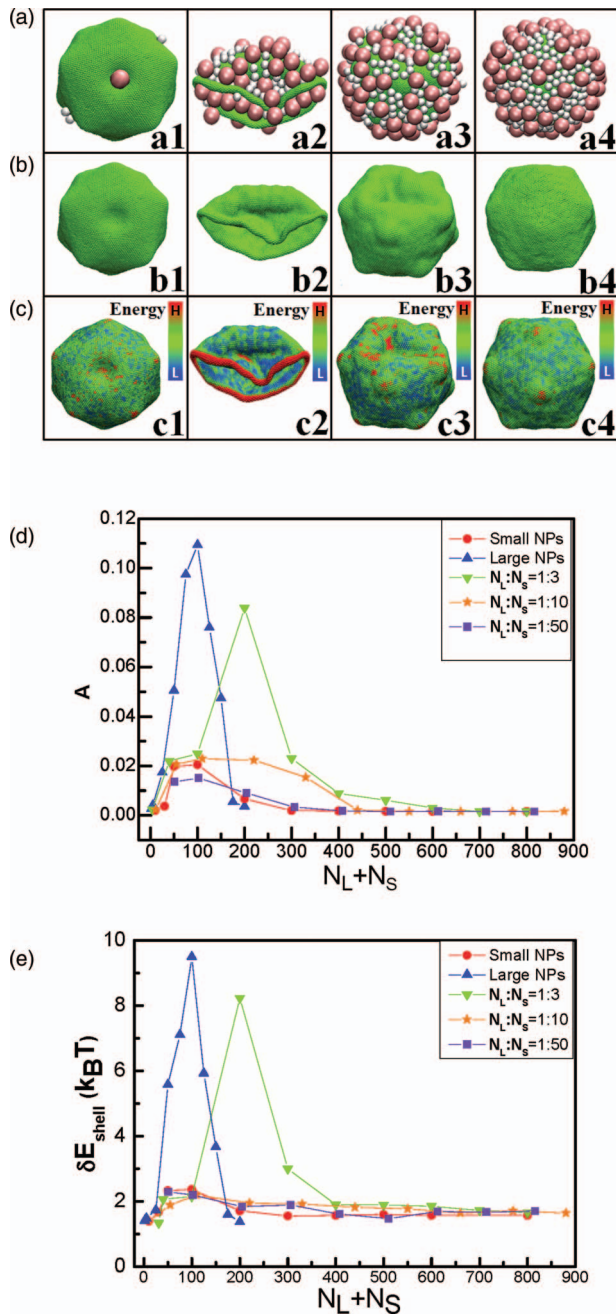


FIG. 5. Snapshots showing the conformations (a) of adsorbed binary NPs, the deformations (b) and the energy maps (c) of elastic shell with the ratio of $N_L:N_S = 1:3$ at $D_0 = 15$ and $K_b = 300$. Different shades correspond to the relative strengths as indicated in the color bar on the right side and from left to right, $N_L + N_S = 4, 200, 400$, and 600 , respectively. The asphericity A (d) and the energy deviation δE_{shell} (e) of elastic shell as a function of the total number of binary NPs $N_L + N_S$ with $N_L:N_S = 1:3, 1:10, 1:50$, pure small NPs, and pure large NPs at $D_0 = 35$ and $K_b = 1000$.

of soft elastic shell is observed (see Fig. 5(a3)). The shape of elastic shell is fully spherical again when the total number of binary NPs increases to $N_L + N_S = 600$, as shown in Fig. 5(a)(a4), which is almost the same as the free elastic shell. To gain insight into the physical origin of shape transitions of elastic shell, we measure the stretching energy and the bending energy at each bead of elastic shell, and the energy maps are shown in Fig. 5(c). When 4 binary NPs are adsorbed on the elastic shell, the effects of adsorbed binary NPs

on the elastic shell are not obvious, the energy fluctuation in energy map is very small, see Fig. 5(c)(c1). While a few binary NPs are adsorbed on the elastic shell, the binary aggregate anisotropically and the distribution of energy including the stretching energy and bending energy is uneven as shown in Fig. 5(c)(c2). The adsorptions of a few binary NPs on elastic shell destroy the symmetry on the shell surface, so the elastic shell is collapsed for this asymmetry. Afterward, if there is sufficient number of binary NPs, the binary NPs are adsorbed uniformly on the shell surface [Fig. 5(b)(a4)], and the shell surface symmetry can be restored [Fig. 5(b)(b4)]. The reason why the spherical shape of shell can appear again may be that the energy for each bead becomes the same and the energy distribution in energy map is uniform, see Fig. 5(c)(c4). In fact, the deformation of elastic shell can be indicated by the asphericity A , which is defined as^{10,15}

$$A = \frac{\langle \Delta R^2 \rangle}{\langle R \rangle^2} = \frac{1}{N_b} \sum_{i=1}^{N_b} \frac{(R_i - \langle R \rangle)^2}{\langle R \rangle^2}, \quad (8)$$

where R_i refers the radial distance of the surface bead i and $\langle R \rangle$ is the mean radius of the elastic shell. Meanwhile, the energy deviation δE_{shell} for beads of soft elastic shell is calculated, and the results are shown in Fig. 5(e). Here the energy deviation δE_{shell} is defined as

$$\delta E_{shell} = \sqrt{\frac{1}{N_b} \sum_{i=1}^{N_b} (E_{i,shell} - \langle E_{shell} \rangle)^2}, \quad (9)$$

where $E_{i,shell}$ refers the energy of the surface bead i , $\langle E_{shell} \rangle$ is the average shell energy per bead, and the shell energy only includes the stretching energy and the bending energy. A small value of δE_{shell} indicates that the energy values for beads all approach to the average value $\langle E_{shell} \rangle$, and the distribution is uniform in energy maps. Take the proportion of $N_L/N_S = 1/3$ as an example. The deformation of soft elastic shell binding with quite few NPs ($N_L + N_S = 4$) is very small because the effects of adsorbed NPs on the soft elastic shell can be ignored, the surface is still almost a sphere, and both the asphericity A and the energy deviation δE_{shell} are very small. When the total number of adsorbed NPs increases, the soft elastic shell collapses gradually, both the asphericity A and the energy deviation δE_{shell} increase and reach the peaks when $N_L + N_S = 200$, see Fig. 5(b)(b3). However, if the total number of adsorbed NPs is large enough to cover the shell surface completely, the excluded volume effects of NPs can induce the soft elastic shells to be isotropic, and two characteristic parameters of A and δE_{shell} both become the small value. Meanwhile, the proportion of binary NPs can affect the reshaping behaviors of elastic shell. We calculate the surface asphericity A and the energy deviation δE_{shell} as a function of total number of adsorbed binary NPs with different proportions and the results are shown in Figs. 5(d) and 5(e). For the system of pure large NPs, the transition from the collapsed shell to the spherical shell is observed with $N_L = 175$. However, for the system of pure small NPs, the transition occurs with $N_S = 300$. The conformations of soft elastic shell can be controlled easily by varying the total number of binary NPs. In fact, direct mechanical

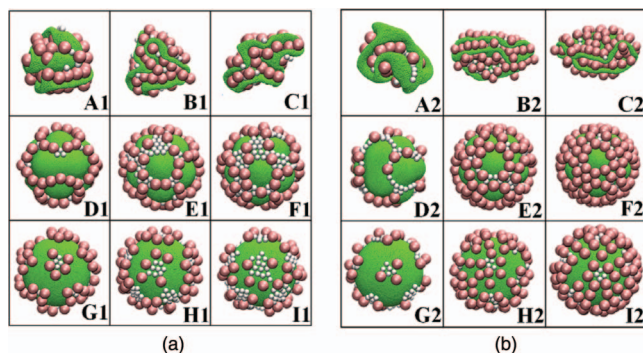


FIG. 6. Snapshots showing the conformations of adsorbed binary NPs with different number of binary NPs. From left to right: (a) $N_S = 30, 90$, and 120 with the number of large NPs fixed $N_L = 60$, and (b) $N_L = 30, 90$, and 120 with the number of small NPs fixed $N_S = 60$. From top to bottom, the bending energy of the elastic shell is $K_b = 200, 1000$, and $20\,000$, respectively.

manipulation can make macroscopic surfaces conform to special shape. However, it is very difficult to use mechanical means to reshape surfaces with very small sizes. In view of those facts, we may provide an effective way to regulate and reshape surfaces with sizes in the micrometer range or smaller.¹²

To explore the effects of the total number of binary NPs and the ratio of large NPs to small NPs on the elastic shell in more detail, we investigate some conformations with different ratios of N_L/N_S . In Fig. 6, from top to bottom, the bending energy of elastic shell is chosen as $K_b = 200, 1000$, and $20\,000$. From left to right, $N_S = 30, 90$, and 120 with the number of large NPs keeps constant $N_L = 60$ in Fig. 6(a), and from left to right, $N_L = 30, 90$, and 120 with the number of small NPs keeps constant $N_S = 60$ in Fig. 6(b). For the elastic shell with $K_b = 200$, the stretching energy of elastic shell loses to the surface pressure caused by adhesion of binary NPs with binding energy $D_0 = 35$ and the elastic shell is collapsed rapidly and completely, see the first rows of Figs. 6(a) and 6(b). At the moderate bending energy $K_b = 1000$, the binary NPs can self-assemble into some fantastic architectures because the lack of small NPs can result in lacking edges of some pentagons, see Fig. 6(a)(D1). While the lack of large NPs also makes the edges empty, and all the vertices are connected, see Fig. 6(b)(D2), in which the system energy approaches to the lowest one. When the number of small NPs increases to 90 and 120 , see Figs. 6(a)(E1) and 6(a)(F1), small NPs aggregate around the vertices and large NPs are located along the edges irregularly. When the number of large NPs increases to 90 and 120 , large NPs can self-assemble into 12 rings around the peaks of elastic shell and small NPs can take up the rest area, see Figs. 6(b)(E2) and 6(b)(F2). When the bending energy become $K_b = 20\,000$, the elastic shell can be treated as a hard shell with a little deformation. Either the number of large NPs or the number of small NPs increases, small NPs are surrounded by large NPs, which makes us believe that the total energy of the system with small NPs inside the clusters is lower than that with large NPs inside the clusters, see the bottom rows of Figs. 6(a) and 6(b). In the competition between small NPs and large NPs, small NPs take advantage in taking over the vertices at the moderate bending energy, which

contributes to the directed self-assembly of binary NPs system and opens an avenue to control the NPs in the nanometer range.

IV. CONCLUSIONS

We investigate the conformations of binary NP adsorbed on the soft elastic shell with using molecular simulations. The conformations of those systems are affected not only by the bending energy of elastic shell and the adhesive strength between binary NPs and elastic shell basically but also by the total number of binary NPs and the ratio of N_L/N_S . At the moderate adhesive strength and bending energy, binary NPs can self-assemble into the ordered regular pentagons, in which the small NPs are located at the vertices of the regular pentagons as well as the large NPs are distributed along the sides of the regular pentagons. The elastic shell is completely collapsed at low bending energy and the binary NPs are aggregated on the surface at high bending energy. Through varying the total number of adsorbed binary NPs on the elastic shell, the shape of the soft elastic shell can be well controlled, which open the avenue for the regulation and reshaping of the soft elastic surfaces in the micrometer range or smaller sizes.

ACKNOWLEDGMENTS

This work was supported by the National Natural Science Foundation of China (Grant Nos. 20974081, 21174131, and 20934004). We are grateful to the reviewers of our paper for their detailed and insightful comments and suggestions.

- ¹P. W. K. Rothmund, *Nature (London)* **440**, 297–302 (2006).
- ²N. P. King, W. Sheffler, M. R. Sawaya, B. S. Vollmar, J. P. Sumida, I. André, T. Gonen, T. O. Yeates, and D. Baker, *Science* **336**, 1171–1174 (2012).
- ³J. D. Hartgerink, E. Beniash, S. I. Stupp, *Science* **294**, 1684–1688 (2001).
- ⁴T. H. Bayburt, Y. V. Grinkova, and S. G. Sligar, *Nano Lett.* **2**, 853–856 (2002).
- ⁵D. Nykypanchuk, M. M. Maye, D. V. D. Lelie, O. Gang, *Nature (London)* **451**, 549–552 (2008).
- ⁶F. Bresme and M. Oettel, *J. Phys.: Condens. Matter* **19**, 413101 (2007).
- ⁷P. Pieranski, *Phys. Rev. Lett.* **45**, 569–572 (1980).
- ⁸K. Zahn and G. Maret, *Phys. Rev. Lett.* **85**, 3656–3659 (2000).
- ⁹A. R. Bausch, M. J. Bowick, A. Cacciuto, A. D. Dinsmore, M. F. Hsu, D. R. Nelson, M. G. Nikolaides, A. Travesset, and D. A. Weitz, *Science* **299**, 1716–1718 (2003).
- ¹⁰A. Šarić and A. Cacciuto, *Soft Matter* **7**, 1874–1878 (2011).
- ¹¹A. Šarić and A. Cacciuto, *Soft Matter* **7**, 8324–8329 (2011).
- ¹²J. C. Pàmies and A. Cacciuto, *Phys. Rev. Lett.* **106**, 045702 (2011).
- ¹³A. Šarić, J. C. Pàmies and A. Cacciuto, *Phys. Rev. Lett.* **104**, 226101 (2010).
- ¹⁴A. Šarić and A. Cacciuto, *Phys. Rev. Lett.* **108**, 118101 (2012).
- ¹⁵D. Zhang, A. H. Chai, X. H. Wen, L. L. He, L. X. Zhang, and H. J. Liang, *Soft Matter* **8**, 2152–2158 (2012).
- ¹⁶W. G. Gelbart, R. P. Sear, J. R. Heath, and S. Chaney, *Faraday Discuss.* **112**, 299–307 (1999).
- ¹⁷R. P. Sear, S.-W. Chung, G. Markovich, W. M. Gelbart, and J. R. Heath, *Phys. Rev. E* **59**, 6255–6258 (1999).
- ¹⁸J. Ruiz-García, R. Gámez-Corralles, and B. I. Ivlev, *Phys. Rev. E* **58**, 660–663 (1998).
- ¹⁹Y. Lin, H. Skaff, T. Emrick, A. D. Dinsmore, and T. P. Russell, *Science* **299**, 226–229 (2003).
- ²⁰F. Li, D. P. Josephson, and A. Stein, *Angew. Chem., Int. Ed.* **50**, 360–388 (2011).
- ²¹A. M. Kalsin, M. Fialkowski, M. Paszewski, S. K. Smoukou, K. J. M. Bishop, B. A. Grzybowski, *Science* **312**, 420–424 (2006).

- ²²E. V. Shevchenko, D. V. Talapin, A. L. Rogach, A. Komowski, M. Haase, and H. Weller, *J. Am. Chem. Soc.* **124**, 11480–11485 (2002).
- ²³N. C. Karayiannis, K. Foteinopoulou, C. F. Abrams, and M. Laso, *Soft Matter* **6**, 2160–2173 (2010).
- ²⁴E. V. Shevchenko, D. V. Talapin, N. A. Kotov, S. O'Brien, and C. B. Murray, *Nature (London)* **439**, 55–59 (2006).
- ²⁵E. V. Shevchenko, D. V. Talapin, C. B. Murray, and S. O'Brien, *J. Am. Chem. Soc.* **128**, 3620–3637 (2006).
- ²⁶Z. Y. Chen, J. Moore, G. Radtke, H. Siringhaus, and S. O'Brien, *J. Am. Chem. Soc.* **129**, 15702–15703 (2007).
- ²⁷P. N. Pusey and W. van Megen, *Nature (London)* **320**, 340–342 (1986).
- ²⁸K. N. Pham, A. M. Puertas, J. Bergenholtz, S. U. Egelhaaf, A. Moussaïd, P. N. Pusey, A. B. Schofield, M. E. Cates, M. Fuchs, and W. C. K. Poon, *Science* **296**, 104–106 (2002).
- ²⁹K. Dawson, G. Foffi, M. Fuchs, W. Götze, F. Sciortino, M. Sperl, P. Tartaglia, Th. Voigtman, and E. Zaccarelli, *Phys. Rev. E* **63**, 011401 (2000).
- ³⁰T. Eckert and E. Bartsch, *Phys. Rev. Lett.* **89**, 125701 (2002).
- ³¹H. Ma and L. L. Dai, *Langmuir* **27**, 508–512 (2011).
- ³²C. W. Hsu and Y. L. Chen, *J. Chem. Phys.* **133**, 034906 (2010).
- ³³S. J. Plimpton, *J. Comput. Phys.* **117**, 1–19 (1995).
- ³⁴S. Nose, *J. Chem. Phys.* **81**, 511 (1984).
- ³⁵W. G. Hoover, *Phys. Rev. A* **31**, 1695–1697 (1985).
- ³⁶See supplementary material at <http://dx.doi.org/10.1063/1.4807592> for more information about the influences of finite size and the size of elastic shell on the self-assembly of binary NPs on soft elastic shells.
- ³⁷G. J. Zarragoicoechea, A. G. Meyra, and V. A. Kuz, *Mol. Phys.* **107**, 549–554 (2009).
- ³⁸A. G. Meyra, G. J. Zarragoicoechea, and V. A. Kuz, *Mol. Phys.* **108**, 1329–1332 (2009).
- ³⁹H. N. W. Lekkerkerker, W. C. K. Poon, P. N. Pusey, A. Stroobants, and P. B. Warren, *Europhys. Lett.* **20**, 559 (1992).
- ⁴⁰D. Zhang, Y. W. Jiang, X. H. Wen, and L. X. Zhang, *Soft Matter* **9**, 1789–1797 (2013).